SCIENTIFIC REPORTS

OPEN

SUBJECT AREAS:
ELECTRONIC MATERIALS
BATTERIES

Received
18 September 2013

Accepted
17 January 2014

Published
5 March 2014

Correspondence and requests for materials should be addressed to Z.Y.W. (wuzy@ustc.edu.cn); W.S.C. (chuws@ustc.edu.cn) or D.G.X. (dgxia@pku.edu.cn)

# Detailed investigation of $Na_{2.24}FePO_4CO_3$ as a cathode material for Na-ion batteries

Weifeng Huang[1,2,3], Jing Zhou[4], Biao Li[2], Jin Ma[2], Shi Tao[1], Dingguo Xia[2], Wangsheng Chu[1] & Ziyu Wu[1,3]

[1]National Synchrotron Radiation Laboratory, University of Science and Technology of China, Hefei, 230029, P. R. China, [2]Key lab of theory and technology for advanced batteries materials, College of Engineering, Peking University, Beijing 100871, P. R. China, [3]Beijing Synchrotron Radiation Facility, Institute of High Energy Physics, Chinese Academy of Sciences, Beijing 100049, P. R. China, [4]Chinese Academy of Sciences, Shanghai Institute Applied Physics, Shanghai 201204, P. R. China.

**Na-ion batteries are gaining an increased recognition as the next generation low cost energy storage devices. Here, we present a characterization of $Na_3FePO_4CO_3$ nanoplates as a novel cathode material for sodium ion batteries. First-principles calculations reveal that there are two paths for Na ion migration along b and c axis. In-situ and ex-situ Fe K-edge X-ray absorption near edge structure (XANES) point out that in $Na_3FePO_4CO_3$ both $Fe^{2+}/Fe^{3+}$ and $Fe^{3+}/Fe^{4+}$ redox couples are electrochemically active, suggesting also the existence of a two-electron intercalation reaction. Ex-situ X-ray powder diffraction data demonstrates that the crystalline structure of $Na_3FePO_4CO_3$ remains stable during the charging/discharging process within the range 2.0–4.55 V.**

Lithium ion batteries (LIBs) represent a real technological advancement in energy storage systems (ESSs), with many applications in our daily life[1–3]: laptops, cameras, mobile phones, *etc.* However, due to the increasing demand of Li for applications in large facilities, the lack of Li resources is a serious drawback. Compared with LIBs, sodium ion batteries (SIBs) appear more appropriate for ESSs because of the abundance of sodium natural resources, its better economic efficiency and the lower cost of raw materials[4–6]. In addition, because of sodium's lower potential for intercalation materials, the electrolyte offers more choices. Compared to standard H electrode, they are −2.71 V for Na+/Na and −3.02 V for Li+/Li, respectively.

Among the investigated cathode materials for SIBs[7–14], polyanionic materials attract a large attention[7,9,14–25], because the main structure contains strong covalent bonds of polyanion characterized by a good thermal stability, which imply improved safety characteristics for these batteries[18,26–30]. Carbonophosphates ($A_3MPO_4CO_3$) introduced by Ceder's team are a good reference for these systems[22,31]. Theoretical works[30,32–34] suggested that the $A_3MPO_4CO_3$ structure can be better deintercalated with more than one Na from crystalline structure, pointing out the existence of a two-electrons reaction. Chen *et al.* successfully synthesized $Na_3MnPO_4CO_3$, and with *ex-situ* solid state NMR experiments, they showed that both $Mn^{2+}/Mn^{3+}$ and $Mn^{3+}/Mn^{4+}$ redox couples are electrochemically active[35]. Actually, the two electrons reaction mechanism implies that electrode materials may have a high specific capacity[31]. However, their effective specific capacity was not good enough, especially at high rates. There are still few reports discussing the factors limiting the capacity or the cycle life. As a consequence, it is still a great challenge enhancing both rate capability and cyclability of $Na_3MnPO_4CO_3$ cathode materials.

In the present work, we used a modified hydrothermal method to synthesize $Na_3FePO_4CO_3$ nanoplates. The structural evolution of this compound was carried out by combining a DFT computation with *in-situ* and *ex-situ* XAS as well as XRD experiments. When used as cathode materials in Na ion batteries, both $Fe^{2+}/Fe^{3+}$ and $Fe^{3+}/Fe^{4+}$ redox are electrochemically active and the crystalline structure remains stable during charging/discharging process. However, when compared with previous works, the as-prepared $Na_3FePO_4CO_3$ system shows better electrochemical properties in terms of both high-rate charge/discharge performance and cyclability[31,35].

## Results

**Geometrical structure and possible $Na^+$ transfer paths.** Figure 1a displays the XRD pattern of the synthesized sample. Diffraction peaks are in good agreement with the standard p21/m space group $Na_3FePO_4CO_3$ (PDF#35-0678). Diffraction features due to impurity were not detected, meanwhile, the strong intensity also suggests a high

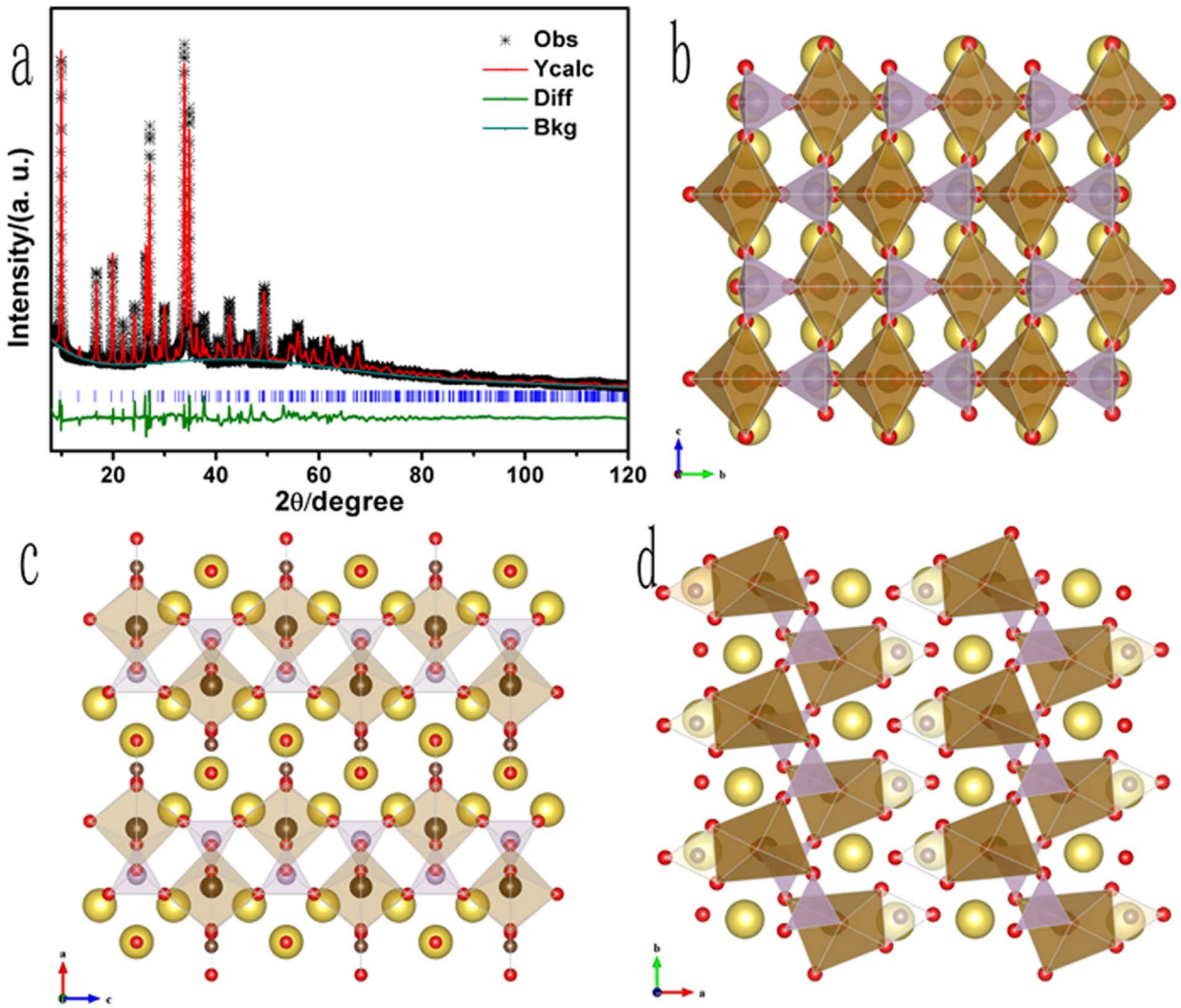


**Figure 1 | Characterization of the geometrical structure.** (a) The XRD Rietveld refinement of the as-prepared $Na_3FePO_4CO_3$ nanoplates; (b–d) geometrical model of the $Na_3FePO_4CO_3$ along the a, b, c axis, respectively. In the model, Na, Fe, P, O and C are yellow, dark brown, purple, red and light brown spheres, respectively. The distorted Fe-O octahedra (dark brown), the P-O tetrahedra (purple) and the C-O plane triangles (light brown) are also shown.

crystallinity of the as-prepared sample. The Rietveld refinement result points out that the accurate molecular formula is $Na_{3-x}FePO_4CO_3$ with a = 8.948334 Å, b = 5.167109 Å, c = 6.593195 Å, β = 90.16091 and V = 304.8485 Å$^3$, as listed in table S1.

Comparison of the white line energy at the Fe K edge among as-prepared $Na_3FePO_4CO_3$, FeO and $Fe_2O_3$ standards supports the existence of a mixed valence between $Fe^{2+}$ and $Fe^{3+}$ configurations (see figure S1). The Mössbauer spectroscopy experiment performed on as-prepared products suggests rewriting the exact formula as $Na_{2.24}FePO_4CO_3$, (see figure S8). However, as proposed in a previous work[31], the crystal structure of the $Na_3FePO_4CO_3$ is isostructural to $Na_3MnPO_4CO_3$ (see figure 1b–d) with a main framework composed of distorted $FeO_6$ octahedra, $PO_4$ tetrahedra and $CO_3$ plane triangles. These groups are connected with each other, forming a two dimensional chain in the (010) plane (see figure 1c). Two different sites (4f and 2e) are present in the crystal for the sodium atoms, named Na1 and Na2, and surrounded by 7 and 6 O atoms, respectively. A first-principles calculation showed that the band gap of the as-prepared $Na_3FePO_4CO_3$ is 3.4 eV, smaller than the value of 3.7 eV of the $LiFePO_4$[36]. The electron density around the Fermi level demonstrates also that $Na_3FePO_4CO_3$ compounds may have a good electronic conductivity (see figure 2a). From figure 2b and 2c, we show also that there are two-dimensional channels along b and c axis to insert Na atoms (Na1-Na2-Na1, Na1-Na1-Na2-Na1), in agreement with a previous report[30]. The energy barriers of two most ideal Na diffusion paths are 0.6 and 0.7 eV (see in table S2), respectively. Both are much higher than the energy barrier of $LiFePO_4$ (0.3 eV)[37], pointing out the low ionic conductivity of the $Na_3FePO_4CO_3$. As a consequence, it is mandatory synthesizing highly oriented nanomaterials along b or c axis to obtain excellent electrochemical performances.

**Morphology and thermostability characterization of $Na_3FePO_4CO_3$.** The morphology and size of as-prepared $Na_3FePO_4CO_3$ products were characterized by transmission electron microscopy (TEM). As shown in figure 3a, TEM images display a plate-like morphology with a width in the range of 100–200 nm and a thickness of ~50 nm. The Brunauer-Emmet-Teller (BET) characterization (see figure S3) demonstrates that the surface area is as high as 46 m$^2$/g and the selected area electron diffraction (SAED) pattern reveals that the exposed planes of $Na_3FePO_4CO_3$ nanoplates have the (001) orientation. As mentioned above, the [001] direction is also one of the Na ion diffusion paths, so that this preferred orientation enhances the Na ion transfer capabilities that results also in a better rate capability.

Figure 3d shows the thermal gravimetric (TG) and differential thermal analysis (DTA) of $Na_3FePO_4CO_3$ nanoplates. Data points

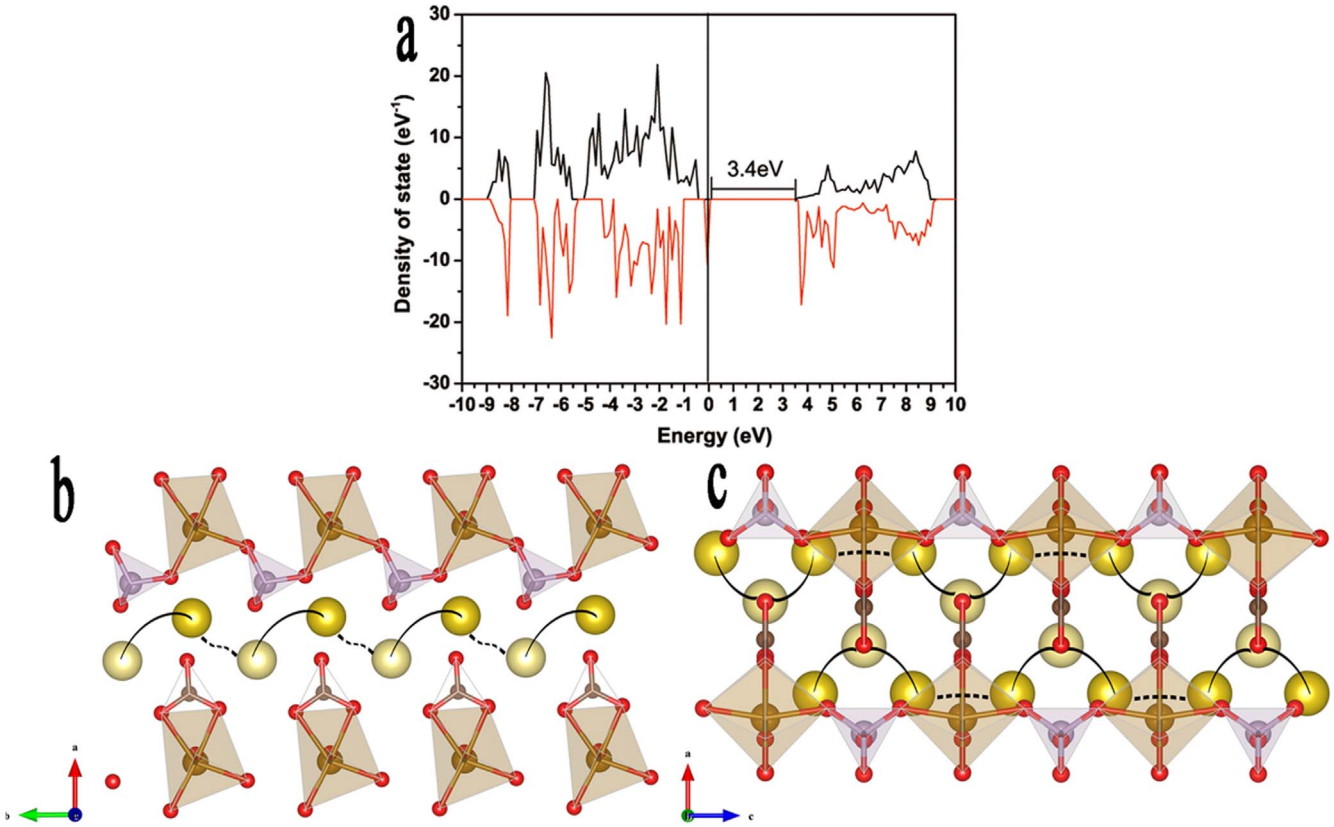


**Figure 2 | The calculated density of state (DOS) and the $Na^+$ transfer paths in the $Na_3FePO_4CO_3$.** (a) The DOS of pure $Na_3FePO_4CO_3$ with GGA + U. The Fermi level is set as a reference; (b) one of the most probable Na diffusion pathways for the $Na_3FePO_4CO_3$ is along the b axis. Its calculated energy barrier is just 0.642 eV; (c) another possible Na diffusion pathway is along the c axis with an energy barrier of 0.716 eV. Dark yellow spheres are 4f Na atoms, light yellow the 2a Na, while solid and dot black lines are the outwards and the inwards diffusion pathways among Na atoms.

out that the material did not experience any thermal decomposition up to 550°C. Moreover, $CO_2$, rather than other flammable gases, would be released even at the decomposition temperature of 550°C. This behavior ensures the safety of SIBs and guarantees the high thermal stability of this cathode candidate, an additional important feature that makes it a suitable cathode material for ESSs.

**Electrochemical characterization of the $Na_3FePO_4CO_3$.** The electrochemical behaviour of the $Na_3FePO_4CO_3$ has been tested with the galvanostatic discharge-charge technique. Figure 4a showed a discharge profile with different cycles at the current density of 10 $mAg^{-1}$ at 20°C (100 mA/g was defined as 1 C). The long plateau at ~2.7 V in the first discharge curve is attributed to the reduction of $Fe^{3+}$ to $Fe^{2+}$. The first discharge capacity can deliver 121 mAh/g. After 50 cycles of test, the capacity still shows a reversible capacity of 96 mAh/g with a columbic efficiency >99%, that represents a really good stability.

Figure 5 shows the first three cyclic voltammogram (CV) curves of the electrodes recorded for the $Na_3FePO_4CO_3$ at the scan rate of 0.1 $mVs^{-1}$ at 20°C. The sample shows a strong peak at around 2.7 V in the first anodic scan that corresponds to a reduction from $Fe^{2+}$ to $Fe^{3+}$ while the broad peaks at ~4.2 V could be associated to the transition from $Fe^{3+}$ to $Fe^{4+}$. In the cathodic scan, two oxidation peaks also occur, accordingly. The two couples of redox features are similar to those of the $Li_2FeSiO_4$ data[39–40], which have been recognized as electrochemically active $Fe^{2+}/Fe^{3+}$ and $Fe^{3+}/Fe^{4+}$ redox. The latter also implies the existence of a possible two electrons reaction path in the $Na_3FePO_4CO_3$.

Regarding $Na_3FePO_4CO_3$ nanoplates, another fundamental improvement is its rate capability. As shown in Figure 4d, the as-prepared $Na_3FePO_4CO_3$ nanoplates showed the highest rate capability among the samples previously reported[35]. Even at the current density of 200 mA/g, $Na_3FePO_4CO_3$ nanoplates still exhibit a favourable specific capacity of 58 mAh/g. Moreover, the $Na_3FePO_4CO_3$ at 10 $mAg^{-1}$ can recover the initial reversible specific capacity after the high rate measurements, implying their good reversibility.

## Discussion

In order to get a deeper understanding of the charge/discharge mechanism and of the structural evolution of the two electrons process, electrochemical tests at different cutoff voltages, in-situ XANES, ex-situ XRD and XANES measurements were carried out. As shown in figure 6, two charge potentials around 2.7 and 4.2 V appear when it is charged to 4.55 V, while we observed only one charge potential for the other charged to 3.8 V. On the other hand, the discharge capacity delivered with 3.8 V cutoff potential was obvious lower than the one charged to 4.55 V. All the different electrochemical performances suggest that further $Na^+$ can be extracted working with a higher voltage. In other words, the $Fe^{3+}/Fe^{4+}$ redox can only be active in a higher potential. A similar situation is found in another polyanionic $Li_2FeSiO_4$ system reported by Yang's team[39].

In-situ XANES spectroscopy and ex-situ XRD were applied to further confirm the occurrence of the two electrons process. The K edge XANES spectroscopy of 3d transition metals originates from an electron excitation from a core level 1s to 4p unoccupied states[41]. Since it is driven by high order correlation functions beyond the pair correlation one, it can be considered a fingerprint of the local geometry around the absorption atoms[42,43]. Moreover, the absorption energy is related to the effective electrons of absorption atoms, so that assuming the same coordination, the energy position shifts to higher level for an increased oxidation state of the absorption atoms. We

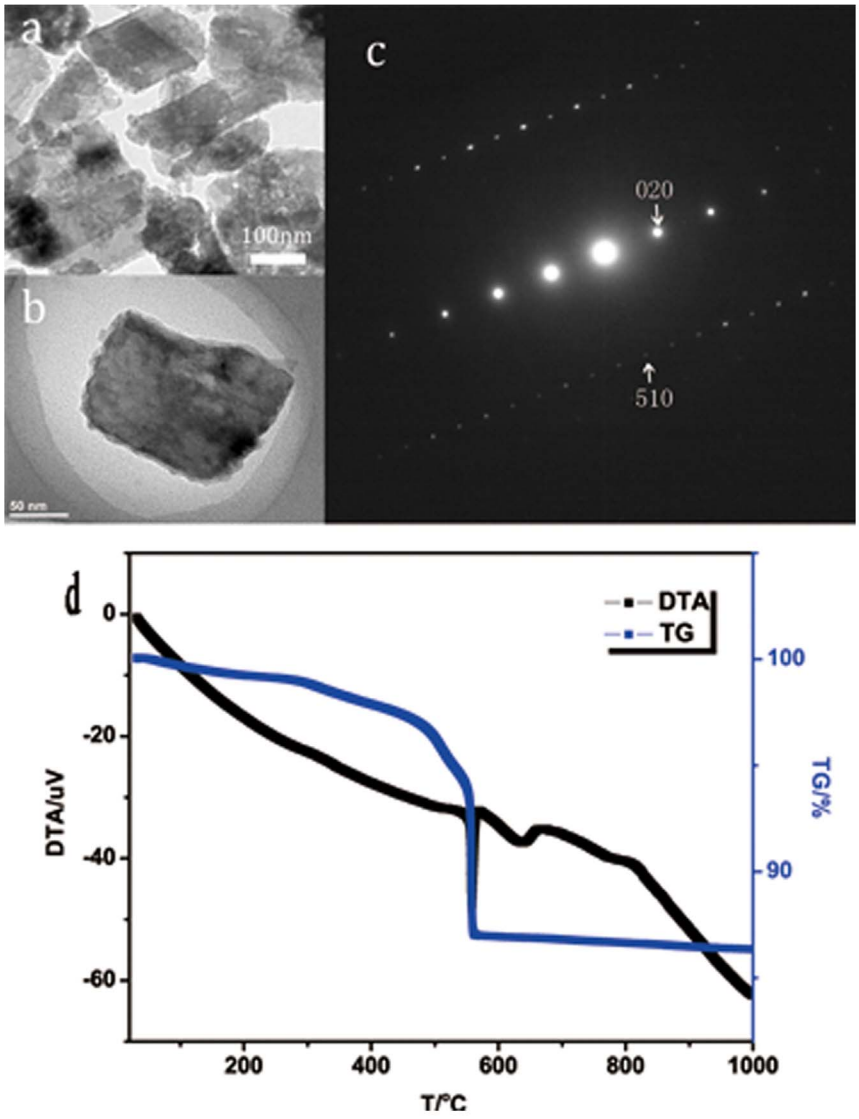


**Figure 3 | TEM, SEAD images and thermostability performance.** (a) A typical TEM image of as-prepared $Na_3FePO_4CO_3$ nanoplates showing the rough plate-like nature; (b) TEM image of a relative smooth nanoplate required for the SEAD analysis, (c) SEAD image of the sample in (b), showing the c axis. (d) Both thermal gravimetric characterization (TG) and differential thermal analysis (DTA) of $Na_3FePO_4CO_3$ nanoplates showing their stability until 550°C.

may then use the shift of the energy position of a XANES spectrum to establish and monitor the change of the valence state. From in-situ XANES spectroscopy showed in figure 7a, we found that both the edge shape and position of the pre-edge do not change, while the energy position shifts to higher energy when charged to 4.55 V. Compared with the reference samples FeO and $Fe_2O_3$, we may claim that the Fe valence state can be increased to a valence higher then 3+ (see figure 7a). On the contrary, for ex-situ experiments, after increasing to $3^+$, figure 7b showed that the Fe valence state remains constant. Because of the instability of the $Fe^{4+}$ it is easy to understand that the $Fe^{4+}$ configuration obtained by the electrochemical reaction can be reduced to $Fe^{3+}$ in air. Therefore, the edge energy position does not shift. Regarding the pre-edge position, we are still unable to fully explain its behavior due to its complexity[38]. However, combined with data available in the literature[13], it is reasonable to consider that the $Fe^{3+}/Fe^{4+}$ redox couple is active.

*Ex-situ* XRD patterns taken with a current of 10 mA/g at different charging/discharging potentials are shown in figure 8. No obvious changes are detectable in the diffraction features of XRD patterns during the Na ion insertion/de-insertion process, suggesting that the charging/discharging is a sing-phase process. The strong intensity of the diffraction peaks indicates also that the cathode material has a stable crystalline structure during the entire charging/discharging process.

The good electrochemical performance of the $Na_3FePO_4CO_3$ nanoplates can be due to: a) a preferred orientation that guarantees a high electrical conductivity of the overall electrode, an improved specific capacity, a good cycling performance and a high rate capability; b) an existing electrochemical active $Fe^{3+}/Fe^{4+}$ redox couple that offers the possibility to obtain a high capacity. As a consequence, the unique characterization of the as-prepared $Na_3FePO_4CO_3$ nanoplates provides a good electrochemical performance when applied to SIBs.

In summary, a simple modified hydrothermal method has been setup to synthesize $Na_3FePO_4CO_3$ nanoplates. A full characterization by SEM, TEM and SEAD revealed that the nanoplate size ranges from 100 to 200 nm with a thickness of about 50 nm. A preferred orientation on the (001) plane has been identified. Moreover, the capacity of $Na_3FePO_4CO_3$ nanoplates stabilized at 96 mAh/g with a current density of 10 mA/g after 50 cycles. Finally, *in-situ* and

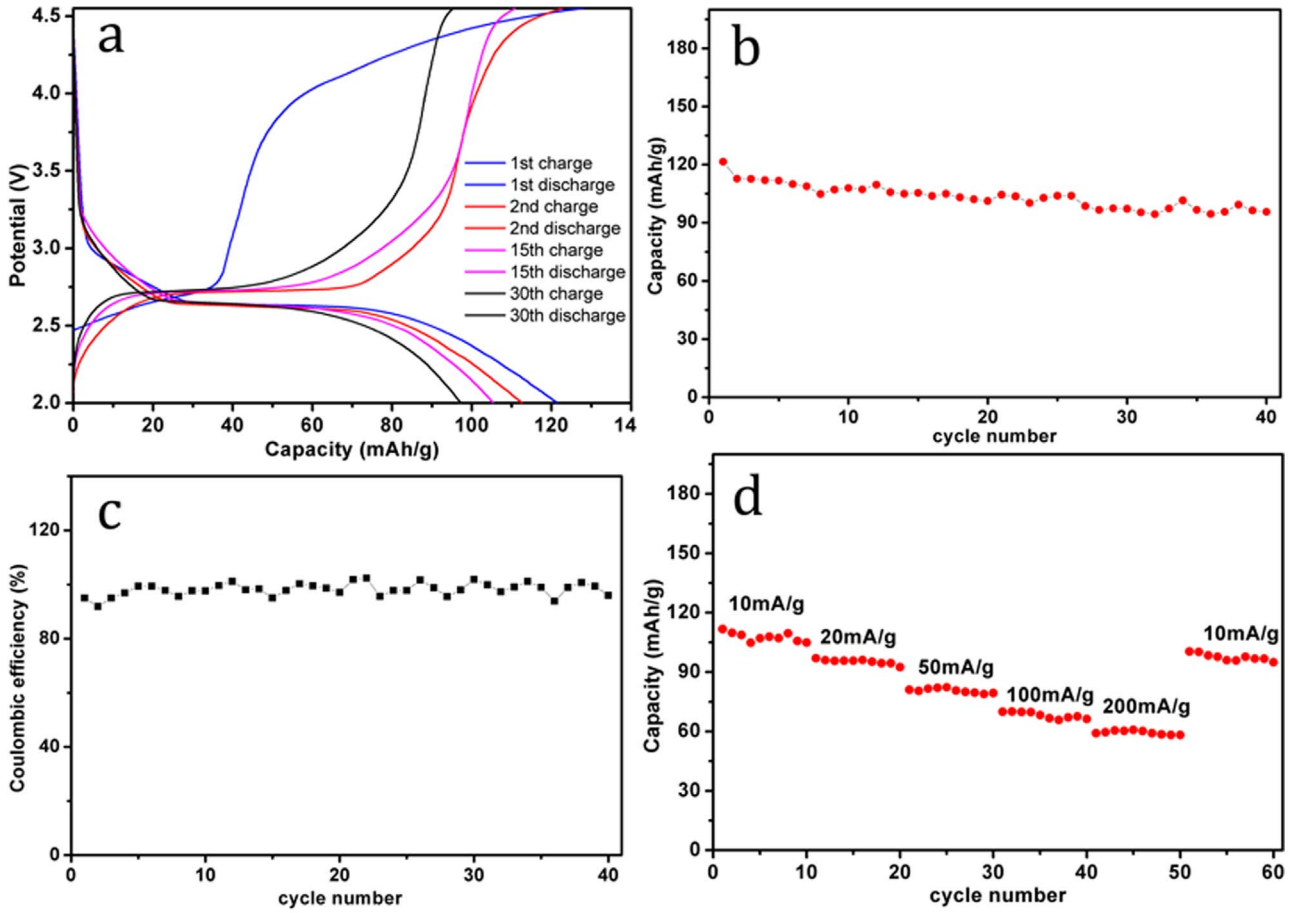


**Figure 4 | Electrochemical performance of the $Na_3FePO_4CO_3$ at RT.** (a) Galvanostatic charge/discharge profiles of $Na_3FePO_4CO_3$ nanoplates at 10 mA/g for different cycles; (b) cycle performance of NIBs at 10 mA/g. (c) Coulombic efficiency of the sample in (b); (d) the rate capability of $Na_3FePO_4CO_3$ nanoplates for different current rates.

*ex-situ* XANES spectroscopy at the Fe K edge provided a direct evidence of the existence of an electrochemical active $Fe^{3+}/Fe^{4+}$ redox. To our knowledge, this is the first systematic evidence of a clear capacity contribution due to $Fe^{2+}/Fe^{3+}$ and $Fe^{3+}/Fe^{4+}$ redox couples. The successful tests performed with the carbonophosphates suggested also that when optimized, polyanion materials could become reliable high-performance and low-cost electrode materials for the next generation of SIBs.

## Methods

**Computational method.** Density functional theory (DFT) calculation was performed using the plane-wave based Vienna ab initio simulation package (VASP)

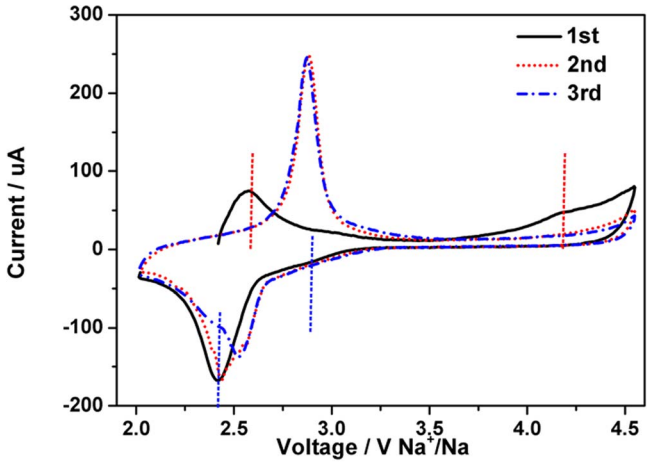


**Figure 5 | CV features.** The cyclic voltammetry (CV) characterization of SIBs with $NaClO_4$ as the electrolyte and metallic Na as the anode. The CV features show a slope potential during the reduction procedure indicating the existence of a $Fe^{3+}/Fe^{4+}$ redox reaction.

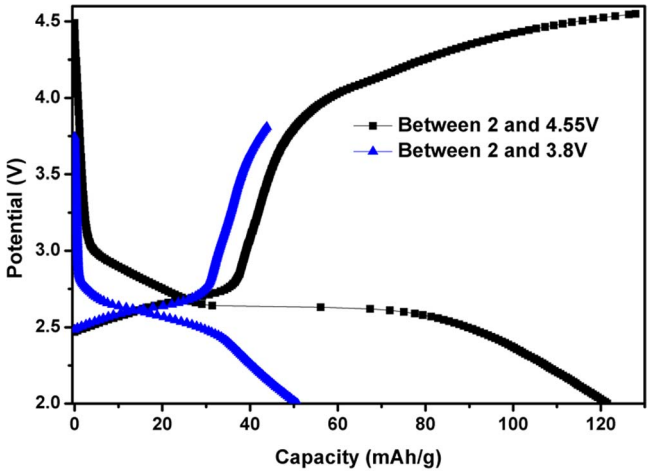


**Figure 6 | Charging/discharging profiles.** Comparison of profiles of as-prepared $Na_3FePO_4CO_3$ nanoplates for a potential in the range 2–3.8 V and 2–4.55 V. Data show different electron contributions during the electrochemical cycle at different cut-off potentials.

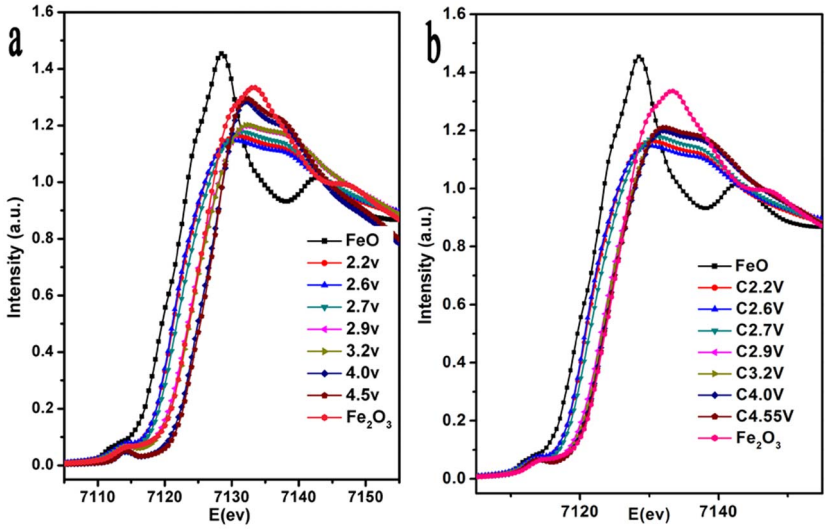


**Figure 7 | In-situ and ex-situ XANES spectroscopy characterization.** (a) in-situ Fe K edge XANES spectroscopy for different charging potentials showing the shift of the edge that probes the Fe valence change. Comparison with the reference samples FeO and $Fe_2O_3$ data point out that the valence may reach a value higher than $3^+$ in the charging process; (b) ex-situ Fe K edge XANES spectroscopy for samples exposed to air. No $Fe^{4+}$ contributions is detected looking at the energy shift.

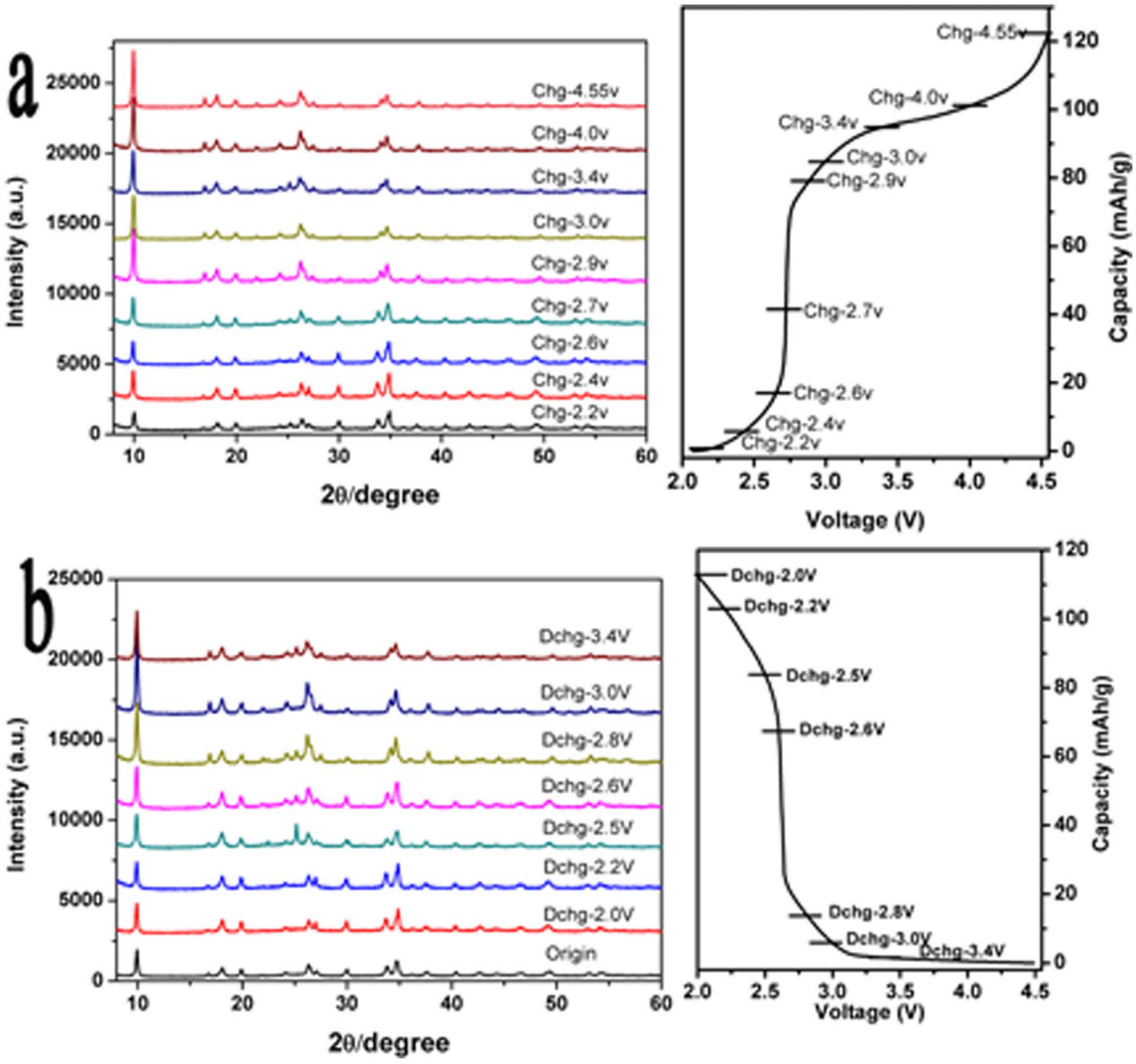


**Figure 8 | XRD characteristics.** (a–b) Ex-situ XRD patterns analysis of $Na_3FePO_4CO_3$ nanoplates during (a) charge and (b) discharge procedures. No structural transformations take place at different potentials during the first cycle. The strong intensity of the diffraction peaks indicates that the cathode material maintains a good crystalline structure during the entire charging/discharging process.

with the generalized gradient approximation (GGA) and exchange correlation functional parametrized by Perdew-Burke-Eernzerhof (PBE). The U parameter for the transition metal Fe is 4.0 eV while the energy cutoff was set to 600 eV for all computations.

**Synthesis of the $Na_3FePO_4CO_3$.** $Na_3FePO_4CO_3$ nanoplates were prepared by a modified hydrothermal method. 4 mmol $FeSO_4.7H_2O$ and 50 mg citric acid were dissolved in 10 ml water/ethylene glycol (EG) mixed solution (volume ratio: $H_2O$/EG = 3/1) to form a clear solution A. After 4 mmol $(NH_4)_2HPO_4$ and 4 g $Na_2CO_3$ were dissolved in 20 ml $H_2O$/EG mixed solution (volume ratio: $H_2O$/EG = 3/1) to form a clear solution B. After a vigorous stirring, the solution A was dropped wisely in the solution B and this mixture was kept stirring for half hour. After that, the mixture products were transferred inside a 40 ml stainless steel autoclave and heated at 180°C for 70 hours. The final products were washed five times by distilled water and dried at 80°C in a vacuum oven overnight.

**Material characterization.** XRD experiments were carried out using an X-ray diffractometer (Bruker D8-Advance) equipped with a Cu Kα radiation (λ = 1.5406 Å). For the Rietveld refinement analysis we scanned over a 2θ range from 8 to 120° at steps of 0.02° for 8 s and data were analyzed using the TOPAS software. Ex-situ XRD data at different voltages during the charging and discharging procedure were collected in a conventional way[29]. To get the desired electrodes, the coin cells, which were charged/discharged to the desired cutoff voltages, needs to be disassembled by an electric criming machine (MTI Co.). Finally, the disassembled electrodes were washed with dimethyl carbonate (DMC), and dried by a hair drier. SEM images recorded by a JEOL 4800 SEM show the sampl morphology. TEM images and SEAD were acquired with a JEM2100F HRTEM. The thermal stability of the samples was evaluated at a heating rate of 5°C/min from RT to 1000°C in air with a TG/DTA thermo-gravimetric analyzer. Fe K edge XANES spectra were recorded at the 1W2B beamline of the Beijing synchrotron radiation facility (BSRF) and at the 14W1B beamline of the Shanghai synchrotron radiation facility (SSRF). For in-situ XAS experiment, coin cells were disassembled in an Ar-filled glove box to take out at first the positive electrode material. To remove the influence of the electrolyte, we cleaned them by DMC solutions. After drying, the positive electrode materials were sealed by a 3 M sellotape in an atmosphere of Ar.

**Electrochemical characterization.** The $Na_3FePO_4CO_3$ nanoplate samples were mixed with carbon (super P) and a Poly tetra fluoro ethylene (PTFE) binder to form a slurry at the weight ratio of 6 : 3 : 1. The mixture was rolled in a thin sheet of uniform thickness (about 40–60 um). After, it was cut in appropriate sections before drying them in a vacuum oven at 120°C for 12 h. The cells were then assembled in an Ar-filled glove box. Metallic Nawas were used as anode for NIBs tests. A high potential electrolyte (purchased from the Beijing Institute of Chemical reagents) with 1 M NaClO4 was used as the electrolyte for NIBs. A separator (whatman) was used for NIB and the charging-discharging performance under different current density was characterized with a cutoff potential in the range 2.0–4.55 V. The cyclic voltammogram was achieved at the scan rate of 0.1 mV/s.


1. Li, H., Wang, Z., Chen, L. & Huang, X. Research on Advanced Materials for Li-ion Batteries. *Adv. Mater.* **21**, 4593–4607 (2009).
2. Goodenough, J. B. & Kim, Y. Challenges for Rechargeable Li Batteries. *Chem. Mater.* **22**, 587–603 (2010).
3. Goodenough, J. B. & Park, K. S. The Li-Ion Rechargeable Battery: A Perspective. *J. Am. Chem. Soc.* **135**, 1167–1176 (2013).
4. Ong, S. P. *et al.* Voltage, stability and diffusion barrier differences between sodium-ion and lithium-ion intercalation materials. *Energ. Environ. Sci.* **4**, 3680–3688 (2011).
5. Palomares, V. *et al.* Na-ion batteries, recent advances and present challenges to become low cost energy storage systems. *Energ. Environ. Sci.* **5**, 5884–5901 (2012).
6. Wang, L. *et al.* A Superior Low-cost Cathode for a Na-ion Battery. *Angew. Chem. Int. Ed.* **52**, 1964–1967 (2013).
7. Ellis, B. L., Makahnouk, W. R., Makimura, Y., Toghill, K. & Nazar, L. F. A multifunctional 3.5 V iron-based phosphate cathode for rechargeable batteries. *Nat. Mater.* **6**, 749–753 (2007).
8. Sauvage, F., Laffont, L., Tarascon, J. M. & Baudrin, E. Study of the insertion/deinsertion mechanism of sodium into $Na_{0.44}MnO_2$. *Inorg. Chem.* **46**, 3289–3294 (2007).
9. Abouimrane, A. *et al.* A new class of lithium and sodium rechargeable batteries based on selenium and selenium-sulfur as a positive electrode. *J. Am. Chem. Soc.* **134**, 4505–4508 (2012).
10. D'Arienzo, M. *et al.* Layered $Na_{0.71}CoO_2$: a powerful candidate for viable and high performance Na-batteries. *PCCP* **14**, 5945–5952 (2012).
11. Qian, J., Zhou, M., Cao, Y., Ai, X. & Yang, H. Nanosized $Na_4Fe(CN)_6$/C Composite as a Low-Cost and High-Rate Cathode Material for Sodium-Ion Batteries. *Adv. Eng. Mater.* **2**, 410–414 (2012).
12. Tepavcevic, S. *et al.* Nanostructured Bilayered Vanadium Oxide Electrodes for Rechargeable Sodium-Ion Batteries. *Acs Nano* **6**, 530–538 (2012).
13. Yabuuchi, N. *et al.* P2-type $Na_{-x}[Fe_{1/2}Mn_{1/2}]O_{-2}$ made from earth-abundant elements for rechargeable Na batteries. *Nat. Mater.* **11**, 512–517 (2012).
14. Lu, Y., Wang, L., Cheng, J. & Goodenough, J. B. Prussian blue: a new framework of electrode materials for sodium batteries. *Chem. Commun.* **48**, 6544–6546 (2012).
15. Barpanda, P. *et al.* Structural, Transport, and Electrochemical Investigation of Novel $AMSO_{(4)}F$ (A = Na, Li; M = Fe, Co, Ni, Mn) Metal Fluorosulphates Prepared Using Low Temperature Synthesis Routes. *Inorg. Chem.* **49**, 7401–7413 (2010).
16. Trad, K. *et al.* $NaMnFe_2(PO_4)_3$Alluaudite Phase: Synthesis, Structure, and Electrochemical Properties As Positive Electrode in Lithium and Sodium Batteries. *Chem. Mater.* **22**, 5554–5562 (2010).
17. Trad, K., Carlier, D., Wattiaux, A., Ben Amara, M. & Delmas, C. Study of a Layered Iron(III) Phosphate Phase $Na_3Fe_3(PO_4)_{(4)}$ Used as Positive Electrode in Lithium Batteries. *J. Electrochem. Soc.* **157**, A947–A952 (2010).
18. Tripathi, R., Ramesh, T. N., Ellis, B. L. & Nazar, L. F. Scalable synthesis of tavorite $LiFeSO_4F$ and $NaFeSO_4F$ cathode materials. *Angew. Chem. Int. Ed.* **49**, 8738–8742 (2010).
19. Zhao, J. *et al.* A novel sol-gel synthesis route to $NaVPO_4F$ as cathode material for hybrid lithium ion batteries. *J. Power Sources* **195**, 6854–6859 (2010).
20. Lee, K. T., Ramesh, T. N., Nan, F., Botton, G. & Nazar, L. F. Topochemical Synthesis of Sodium Metal Phosphate Olivines for Sodium-Ion Batteries. *Chem. Mater.* **23**, 3593–3600 (2011).
21. Barpanda, P. *et al.* Sodium iron pyrophosphate: A novel 3.0V iron-based cathode for sodium-ion batteries. *Electrochem. Commun.* **24**, 116–119 (2012).
22. Chen, H., Hautier, G. & Ceder, G. Synthesis, computed stability, and crystal structure of a new family of inorganic compounds: carbonophosphates. *J. Am. Chem. Soc.* **134**, 19619–19627 (2012).
23. Jain, A. *et al.* A Computational Investigation of $Li_9M_3(P_2O_7)_3(PO_4)_2$ (M = V, Mo) as Cathodes for Li Ion Batteries. *J. Electrochem. Soc.* **159**, A622 (2012).
24. Kang, J. *et al.* High rate performance of a $Na_3V_2(PO_4)_3$/C cathode prepared by pyro-synthesis for sodium-ion batteries. *J. Mater. Chem.* **22**, 20857 (2012).
25. Kim, H. *et al.* New iron-based mixed-polyanion cathodes for lithium and sodium rechargeable batteries: combined first principles calculations and experimental study. *J. Am. Chem. Soc.* **134**, 10369–10372 (2012).
26. Ellis, B. L., Makahnouk, W. R. M., Rowan-Weetaluktuk, W. N., Ryan, D. H. & Nazar, L. F. Crystal Structure and Electrochemical Properties of $A_2MPO_4F$ Fluorophosphates (A = Na, Li; M = Fe, Mn, Co, Ni)†. *Chem. Mater.* **22**, 1059–1070 (2010).
27. Trad, K. *et al.* Structural study of the $Li_{(0.5)}Na_{(0.5)}MnFe_2(PO_4)_3$ and $Li_{(0.75)}Na_{(0.25)}MnFe_2(PO_4)_3$ alluaudite phases and their electrochemical properties as positive electrodes in lithium batteries. *Inorg. Chem.* **49**, 10378–10389 (2010).
28. Liu, Y. *et al.* Porous amorphous $FePO_4$ nanoparticles connected by single-wall carbon nanotubes for sodium ion battery cathodes. *Nano Lett.* **12**, 5664–5668 (2012).
29. Shakoor, R. A. *et al.* A combined first principles and experimental study on $Na_3V_2(PO_4)_2F_3$ for rechargeable Na batteries. *J. Mater. Chem.* **22**, 20535 (2012).
30. Zelang, J. *et al.* Carbon coated $Na_3V_2(PO_4)_3$ as novel electrode material for sodium ion batteries. *Electrochem. Commun.* **14**, 86–89 (2012).
31. Chen, H. *et al.* Carbonophosphates: A New Family of Cathode Materials for Li-Ion Batteries Identified Computationally. *Chem. Mater.* **24**, 2009–2016 (2012).
32. Hautier, G., Fischer, C. C., Jain, A., Mueller, T. & Ceder, G. Finding Nature's Missing Ternary Oxide Compounds Using Machine Learning and Density Functional Theory. *Chem. Mater.* **22**, 3762–3767 (2010).
33. Hautier, G. *et al.* Novel mixed polyanions lithium-ion battery cathode materials predicted by high-throughput ab initio computations. *J. Mater. Chem.* **21**, 17147 (2011).
34. Hautier, G., Ong, S., Jain, A., Moore, C. & Ceder, G. Accuracy of density functional theory in predicting formation energies of ternary oxides from binary oxides and its implication on phase stability. *Phys. Rev. B* **85** (2012).
35. Chen, H. *et al.* Sidorenkite ($Na_3MnPO_4CO_3$): A New Intercalation Cathode Material for Na-Ion Batteries. *Chem. Mater.* **25**, 2777–2786 (2013).
36. Wang, Z. L. *et al.* Investigation of Electronic Conductivity and Occupancy Sites of Mo Doped into $LiFePO_4$ by ab Initio Calculation and X-ray Absorption Spectroscopy. *J Phys. Chem. C* **112**, 17450–17455 (2008).
37. Dathar, G. K. P., Sheppard, D., Stevenson, K. J. & Henkelman, G. Calculations of Li-Ion Diffusion in Olivine Phosphates. *Chem. Mater.* **23**, 4032–4037 (2011).
38. Westre, T. E. *et al.* A multiplet analysis of Fe K-edge 1s->3d pre-edge features of iron complexes. *J. Am. Chem. Soc.* **119**, 6297–6314 (1997).
39. Lv, D. *et al.* A novel $Li_2FeSiO_4$/C composite: Synthesis, characterization and high storage capacity. *J. Mater. Chem.* **21**, 9506 (2011).
40. Lv, D. *et al.* Understanding the High Capacity of $Li_2FeSiO_4$: In Situ XRD/XANES Study Combined with First-Principles Calculations. *Chem. Mater.* **25**, 2014–2020 (2013).
41. Huang, W.-F. *et al.* Investigation of Structural and Magnetic Properties of CoPt/CoAu Bimetallic Nanochains by X-ray Absorption Spectroscopy. *J Phys. Chem. C* **117**, 6872–6879 (2013).
42. Zhang, L. *et al.* Regulation of Magnetic Behavior and Electronic Configuration in Mn-Doped ZnO Nanorods through Surface Modifications. *Chem. Mater.* **24**, 1676–1681 (2012).
43. Zhang, L. J. *et al.* High-Tc ferromagnetism in a Co-doped ZnO system dominated by the formation of a zinc-blende type Co-rich ZnCoO phase. *Chem. Commun.* **48**, 91–93 (2012).


## Acknowledgments

Authors acknowledge Dr. Lin and Dr. Li of the Shanghai Institute of Applied Physics for their kind help on the Mossbauer experiment. This work was partly supported by the

National Basic Research Program of the Ministry of Science & Technology of China (2012CB825800), the Science Fund for Creative Research Groups, NSFC (11321503), the Knowledge Innovation Program of the Chinese Academy of Sciences (KJCX2-YW-N42), the major program of the Beijing Municipal Natural Science Foundation (No.2110001) and the National Natural Science Foundation of China (NSFC 10805055, 11179023,11275227, U1232131 and No.11179001). We sincerely acknowledge the staff of the XAS beamlines of the Beijing Synchrotron Radiation Facility and of the Shanghai Synchrotron Radiation Facility for their support.

## Author contributions

D.X. and Z.W. designed the experiments. W.H., B.L., J.M. and S.T. performed experiments and data analysis. J.Z., W.H., W.C. and Z.W. pformed the calculations. D.X. and Z.W. led the whole work and the analysis. W.H., D.X. and Z.W. wrote the text.

## Additional information

**Supplementary information** accompanies this paper at http://www.nature.com/scientificreports

**Competing financial interests:** The authors declare no competing financial interests.

**How to cite this article:** Huang, W.F. *et al.* Detailed investigation of $Na_{2.24}FePO_4CO_3$ as a cathode material for Na-ion batteries. *Sci. Rep.* **4**, 4188; DOI:10.1038/srep04188 (2014).